Nanoscale Research Letters
a SpringerOpen Journal

NANO EXPRESS   **Open Access**

Large-scale and uniform preparation of pure-phase wurtzite GaAs NWs on non-crystalline substrates

Ning Han[1], Jared J Hou[1], Fengyun Wang[1], SenPo Yip[1], Hao Lin[1], Ming Fang[1], Fei Xiu[1], Xiaoling Shi[1], TakFu Hung[1] and Johnny C Ho[1,2*]

Abstract

One of the challenges to prepare high-performance and uniform III-V semiconductor nanowires (NWs) is to control the crystal structure in large-scale. A mixed crystal phase is usually observed due to the small surface energy difference between the cubic zincblende (ZB) and hexagonal wurtzite (WZ) structures, especially on non-crystalline substrates. Here, utilizing Au film as thin as 0.1 nm as the catalyst, we successfully demonstrate the large-scale synthesis of pure-phase WZ GaAs NWs on amorphous SiO_2/Si substrates. The obtained NWs are smooth, uniform with a high aspect ratio, and have a narrow diameter distribution of 9.5 ± 1.4 nm. The WZ structure is verified by crystallographic investigations, and the corresponding electronic bandgap is also determined to be approximately 1.62 eV by the reflectance measurement. The formation mechanism of WZ NWs is mainly attributed to the ultra-small NW diameter and the very narrow diameter distribution associated, where the WZ phase is more thermodynamically stable compared to the ZB structure. After configured as NW field-effect-transistors, a high I_{ON}/I_{OFF} ratio of $10^4 - 10^5$ is obtained, operating in the enhancement device mode. The preparation technology and good uniform performance here have illustrated a great promise for the large-scale synthesis of pure phase NWs for electronic and optical applications.

Keywords: GaAs nanowires, Wurtzite phase, Non-crystalline substrates, P-type semiconductors

PACS: 61.46.Km, 73.63.Nm, 78.40.Fy

Background

Due to the outstanding chemical and physical properties, III-V compound semiconductor nanowire (NW) materials such as InAs and GaAs are considered to be one of the most promising candidates for next-generation electronics and photonics [1-4]. Typically, they are synthesized *via* metal-catalyzed (e.g., Au, Ni) vapor–liquid-solid (VLS), and/or vapor-solid-solid (VSS) processes in metalorganic chemical vapor deposition (MOCVD) or molecular beam epitaxy (MBE) systems. During the growth, the temperature, V/III ratio, catalyst dimension, and other processing parameters can be precisely varied, aiming to control the crystal quality and growth orientation of

NWs [5-9], in which the corresponding electrical and optical properties can then be tailored for various technological applications.

Since the cubic zincblende (ZB) crystal structure is more energy-stable than the hexagonal wurtzite (WZ) one in most of the bulk III-V semiconductors, the WZ structure is commonly observed as crystal defects (stacking faults and twin planes) in NWs due to the surface energy change in the nanometer scale [10,11]. Notably, pure WZ-structured NWs are only observed with small diameters (approximately 10 nm) [12]. These crystal defects are detrimental to electronic and optical properties of NWs; for example, the mixed phase InAs NWs have a resistivity up to 2 orders of magnitude higher than that of single phase NWs [13], and the electron mobility is found to decrease significantly in highly defective InAs and InP segments [14,15]. In general, the pure phase NWs can be prepared by controlling the

* Correspondence: johnnyho@cityu.edu.hk
[1]Department of Physics and Materials Science, City University of Hong Kong, 83 Tat Chee Ave., Hong Kong, SAR 999077, China
[2]Centre for Functional Photonics (CFP), City University of Hong Kong, 83 Tat Chee Ave., Hong Kong, SAR 999077, China

Springer

basic growth parameters in MOCVD or MBE system, in which the low growth temperature and high V/III ratio favor the ZB structure, while the reverse condition is preferred for the WZ structure [5-7]. Even though the WZ structure dominates in the growth of thin NWs, the thick WZ ones can still be achieved by the lateral growth of firstly prepared thin WZ NWs with the tapering morphology and low defect density [12] at a high V/III ratio of 200. At the same time, single-crystalline wafers such as GaAs(111)B and InAs(111)B are usually used as substrates for the epitaxial growth of NWs. Nowadays, non-crystalline substrates are highly preferred as to lower the preparation cost and to ease the subsequent NW integration by assembling NW parallel arrays [16-18]. However, since Au/GaAs(111)B interface favors the WZ stacking while Au/GaAs(111)A interface favors the ZB structure [19], it is understood that it is even more difficult to achieve pure phase NWs on non-crystalline substrates, without the underlying lattice, which guides the formation of NWs. As a result, controlling the crystal structure of III-V NWs for the pure-phase and uniform property in the large scale is still a challenging topic.

Herein, in this work, pure-phase WZ GaAs NWs are successfully prepared on non-crystalline SiO_2/Si substrates in the large scale by just controlling the NW diameter in the order of approximately 10 nm. XRD patterns show the first observation of pure WZ phase NWs grown on amorphous substrates in the literature, while the electronic bandgap determined by the reflectance spectra fits well with the relatively larger bandgap of WZ phase as compared to the one of ZB structure. Excellent electronic properties are also revealed after configuring the NW as a field-effect-transistor (FET).

Methods

Synthesis of GaAs NWs

A dual-zone horizontal tube furnace, one zone for the solid source (upstream) and one zone for the sample (downstream), was used as the reactor for the synthesis of GaAs NWs, as reported previously [17]. At first, thermal evaporation was carried out with 99.995% pure Au to deposit a 0.1-nm thick Au film on SiO_2/Si substrates (50 nm thermally grown) under a vacuum of approximately 1×10^{-6} Torr. The processed substrate was then placed in the middle of the downstream zone with a tilt angle of approximately 20° and thermally annealed at 800°C for 10 min in a hydrogen environment to obtain Au nanoclusters as the catalysts. The solid source, GaAs powders (approximately 1.0 g), placed within a boron nitride crucible, was positioned in the upstream zone with a distance of 10 cm away from the sample. During the NW growth, the source was heated to the required source temperature (900°C), while the substrate was

cooled to the preset growth temperature (580°C to 620°C). Hydrogen (99.9995% purity, 100 sccm) was used as the carrier gas to transport the thermally vaporized solid GaAs source to the downstream, and the pressure was maintained at approximately 0.5 Torr for the entire duration of the growth (1 h). After the growth, the source and substrate heater were stopped together and cooled down to room temperature under the hydrogen flow. In this case, the NWs were grown chemically intrinsic without any intentional dopants.

Characterization of GaAs NWs

Surface morphologies of the grown GaAs NWs were examined with a scanning electron microscope (SEM, FEI Company, Oregon, USA/Philips XL30, Philips Electronics, Amsterdam, The Netherlands) and transmission electron microscope (TEM, Philips CM-20). Crystal structures were determined by collecting X-ray diffraction (XRD) patterns on a Philips powder diffractometer using Cu Kα radiation (λ = 1.5406 Å), imaging with a high resolution TEM (JEOL 2100F, JEOL Co., Ltd., Tokyo, Japan), and selected area electron diffraction (SAED, Philips CM-20). Elemental mappings were performed using an energy dispersive X-ray detector attached to the JEOL 2100F to measure the chemical composition of grown NWs. For the elemental mapping and TEM, the GaAs NWs were first suspended in the ethanol solution by ultrasonication and drop-casted onto the grid for the corresponding characterization. The reflectance spectrum was measured with a Lambda 750 spectrophotometer (PerkinElmer Inc., MA, USA) at room temperature.

The GaAs NWFETs were fabricated by drop-casting the NW suspension onto highly doped p-type Si substrates with a 50-nm thermally grown gate oxide. Photolithography was utilized to define the source and drain regions, and 50-nm thick Ni film was thermally deposited as the contact electrodes followed by a lift-off process. Electrical performance of fabricated back-gated FETs was characterized with a standard electrical probe station and Agilent 4155C semiconductor analyzer (Agilent Technologies, CA, USA).

Results and discussion

As shown in Figure 1, SEM and TEM images depict the surface morphology of GaAs NWs grown by the 0.1-nm thick Au catalyst film, where they all have a smooth surface, high aspect ratio, and uniform diameter along the entire length of NWs. The NW diameter distribution is carried out by measuring approximately 100 NWs in the TEM images, and the statistics shows an average diameter of 9.5 ± 1.4 nm. All of these have demonstrated a
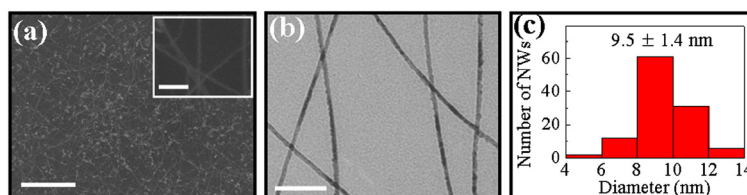
Figure 1 SEM and TEM images depict the surface morphology of GaAs NWs. (**a**) SEM image (scale bar = 2 μm) and magnified image in the inset (scale bar = 100 nm) and (**b**) TEM image (scale bar = 100 nm) of GaAs NWs grown by 0.1-nm thick Au film. (**c**) NW diameter distribution statistics performed in (b) is plotted after a measurement of approximately 100 NWs in TEM images.

narrow diameter distribution utilizing this simple growth technique on non-crystalline substrates. Notably, the XRD pattern in Figure 2a agrees well with the WZ-structured GaAs (PDF 01-080-0003), which illustrates that the NWs were predominantly (>95% considering the resolution of XRD) grown in the pure WZ phase in the large scale. Furthermore, the SAED pattern of one typical NW (Figure 2b) is presented in Figure 2c, where the pattern also fits well with the hexagonal structure, and the specific NW is identified to grow in $<11\bar{2}2>$ direction.

To further study the crystal structure of grown GaAs NWs in detail, HRTEM images are obtained, and one typical NW is shown in Figure 3. A spherical catalytic tip is obviously observed in Figure 3a inferring a VLS/VSS growth mechanism of the GaAs NWs [8,20]. As verified by the EDS spectra (Figure 3b), the catalytic tip consists mainly of the Au and Ga constituents, with an atomic ratio approximating 1:1, and with neglectable concentration of As. This can be explained by the widely accepted VLS/VSS growth mechanism that Ga precursors come from the diffusion and precipitation of Au-Ga alloy tips, and As precursors are mainly provided from the ambient vapor, because of the low solubility of As in Au [8,20,21], reacting with Ga at the NW tip and body interface to yield NWs. The fast Fourier transform (FFT) of the Au-Ga alloy tip (Figure 3a inset) shows the crystal structure of the AuGa crystal viewed from $[\bar{1}22]$ direction, which well agrees with that of the standard AuGa alloy (PDF 3-065-1488); therefore, the GaAs NW is

found catalyzed by the orthorhombic structured AuGa alloy, assuming no post-growth as the growth is stopped instantaneously with no Ga and As precursor supply. In the meanwhile, the HRTEM image in Figure 3c shows a good crystallinity of the NW body, with spacings of 0.32 and 0.34 nm, fitting well with those of {0002} and {10$\bar{1}$0} planes, and the WZ structure is again verified by the FFT presented in the inset viewed from $[2\bar{1}\bar{1}0]$ direction. It is also noted that the growth direction of NWs is <0001> in Figure 3c, which is different from that of Figure 2b showing a mixed growth orientations in these NWs. Moreover, as indicated from the EDS spectrum (Figure 3d), the Ga/As ratio approximates 1:1, suggesting the stoichiometric composition of the grown NWs. Notably, a small amount of oxygen (approximately 5 atomic%) is also identified in the spectrum, which mainly comes from the amorphous surface oxide as shown in Figure 3c. The oxide surface (approximately 2 nm thick) would provide a high concentration of trap states in the interface of oxide/NW, which influences the electronic properties of GaAs NWs as we reported earlier [22], and will also be discussed in details in the following sections.

In this case, all the crystallographic studies have verified the WZ structure of GaAs NWs grown by 0.1-nm thick Au catalyst film deposited on non-crystalline substrates. Without the guidance of underlying crystalline lattice, the obtained pure WZ phase is mainly attributed to the ultra-small NW diameter and the very narrow distribution associated as shown in Figure 1c. It is
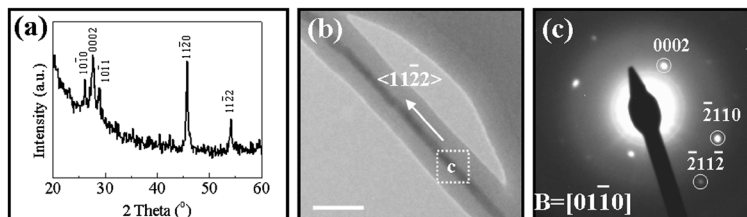

Figure 2 XRD pattern of GaAs NWs and the TEM images of the corresponding SAED pattern. (**a**) XRD pattern of GaAs NWs grown by 0.1-nm thick Au film on SiO$_2$/Si substrates showing the wurtzite structure; (**b**) and (**c**) are the TEM images (scale bar = 50 nm) and the corresponding SAED pattern of one typical NW showing the WZ phase and growth orientation of $<11\bar{2}2>$.
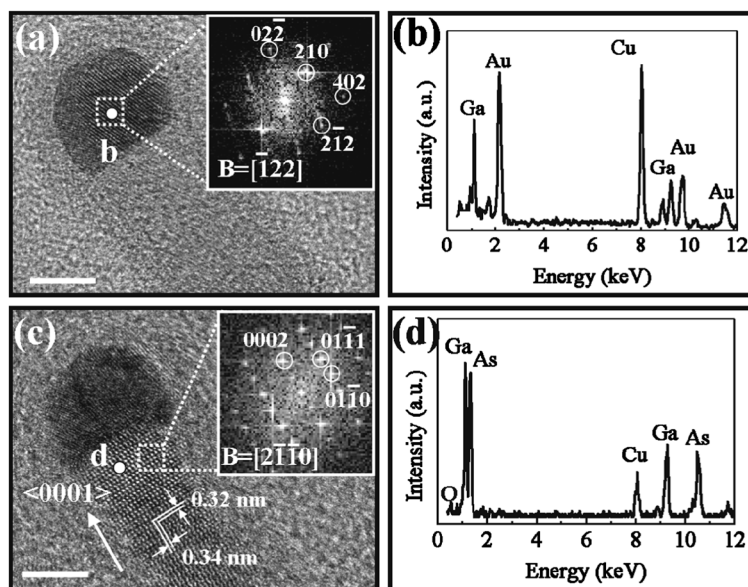
Figure 3 HRTEM, the corresponding FFT images and EDS spectra. (**a**) and (**c**) are the HRTEM images and the corresponding FFT (insets) of the catalyst tip and NW body (scale bar = 5 nm); (**b**) and (**d**) are the EDS spectra of the catalyst tip and NW body in (a) and (c), respectively. It is also noted that the FFT of NW body in (a) is shown in (c) as the tip and the body are not observed under the same zone axis.

commonly believed that the WZ phase is more preferred in small diameter III-V NWs due to the thermodynamically lower energy surfaces. Although the ZB phase is favored in the bulk material, when the materials are scaled down to the nanometer, there exists a transition regime where the dominant ZB phase is replaced by the WZ structure. NWs with the diameter of approximately 10 to 25 nm for GaAs and approximately 50 to 60 nm for InAs are reported as the critical diameters for this transition in the literature [11,12,23-25]. Consequently, as most of our NWs are grown in the diameter <14 nm (mean = 9.5 nm), well below the critical diameter, it is predictable that all NWs existed in the WZ phase on amorphous substrates.

To shed light to explore the electronic bandgap of prepared GaAs NWs, reflectance measurement is performed, and the typical spectrum is shown in Figure 4. It is obvious that the incident light with a wavelength of <765 nm is mostly absorbed by GaAs NWs and thus has the lower reflectance intensity; this way, a bandgap (E_g) of approximately 1.62 eV can be estimated. It is well accepted that the bandgap will be blue-shifted when the diameter of NWs is smaller than 20 nm, and a bandgap of 1.5 to 1.65 eV is usually determined in thin NWs in the literature [26-30]. As the bandgap of WZ GaAs is about 20 to 30 meV higher than that of the ZB GaAs [27,31], it is plausible that our WZ GaAs NWs have a bandgap of approximately 1.62 eV. It is also noted that no photoluminescence can be observed in our NWs which might be due to the trap states in

the oxide/NW interface providing the recombination centers for the non-radioactive recombination of electron/holes pairs.

At the same time, corresponding electrical properties are also investigated by fabricating the as-grown NWs into the back-gated FET, with one representative SEM image and the configuration scheme depicted in Figure 5a. As discussed above, there is a native oxide shell (approximately 2 nm thick) surrounding the GaAs NW, which provides electron trap states and then
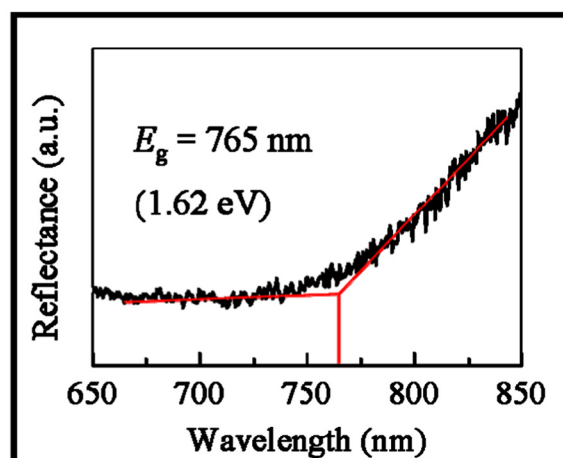

Figure 4 Typical reflectance spectrum. Reflectance spectrum (black line) of the GaAs NWs grown by 0.1-nm thick Au film on SiO$_2$/Si substrates, which determines the electronic bandgap (E_g) of approximately 1.62 eV by extrapolation (red line).
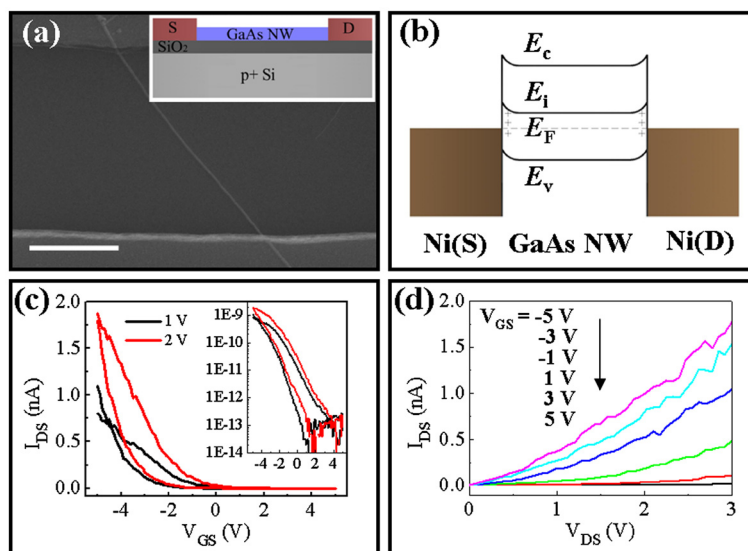
Figure 5 SEM image, band diagram, I_{DS}-V_{GS}, and I_{DS}-V_{DS} curves. (a) SEM image (scale bar = 1 μm) of one representative NW FET; the inset shows the schematic illustration of the back-gated FET configuration. (b) Band diagram of the NWs contacted with Ni source/drain electrodes. (c) I_{DS}-V_{GS} curves and (d) I_{DS}-V_{DS} curves of the NW FET.

depletes the electrons in the GaAs NW core [32,33]. Typically for our unintentionally doped GaAs NWs, the ones with diameters below 40 nm would be fully depleted as to make a p-type semiconductor, while thick NWs are lightly depleted to persist the native n-type characteristics [22]. As a result, all the small-diameter WZ NWs exhibit typical p-type behaviors as shown in Figure 5c, where the I_{DS}-V_{GS} curves show the high ON/OFF current ratio (I_{ON}/I_{OFF}) of 10^4 to 10^5 operating in the enhancement mode, even though the ON current is relatively low in the magnitude of 10^{-9} A. The I_{DS}-V_{DS} curves in Figure 5d show a quasi-ohmic contact of the NW with Ni source/drain electrodes. In the ideal contact of Ni with clean GaAs surface, there should be a high Schottky barrier, theoretically considering the high work function of Ni approximately 5.2 eV and the low electron affinity of GaAs approximately 4.07 eV [34]. However, as the NW is fully depleted by the trapping states, the bands are all pushed upwards, and the oxide shell outside the GaAs NW would pin the Fermi level (E_F) at approximately 1/3 E_g above valence band (E_v) regardless of the metal used [35], as shown in the band diagram (Figure 5b). Consequently, the Schottky barrier becomes significantly smaller and thus makes the Ni-GaAs NW quasi-ohmic contacts.

Conclusions

In summary, the high aspect ratio, smooth, large-scale, and uniform WZ GaAs NWs are prepared on non-crystalline SiO_2/Si substrate, utilizing 0.1-nm thick Au film as the catalyst. The WZ structure is verified by specific characteristics in the XRD pattern, SAED pattern,

HRTEM, and FFT. The electronic bandgap is also determined to be approximately 1.62 eV by the reflectance measurement. Notably, the WZ GaAs NWs all exhibit p-type semiconducting behavior with a high I_{ON}/I_{OFF} ratio of 10^4 to 10^5, as revealed from the electrical characterization in fabricated back-gated NWFETs. All of these have demonstrated the successful control of pure WZ NWs grown on non-crystalline substrates, which present the potency of large-scale preparation for various high performance technological applications.

Authors' contributions
NH prepared the NWs and drafted the manuscript. JJH fabricated the NWFET, and SY made the I-V measurement. FW made the SEM and TEM observations, and HL calculated the NW diameter distribution. MF carried out the XRD measurement, and FX made the SAED identification. XS carried out the reflectance spectrum, and TH observed the HRTEM and EDS. JCH provided the idea and completed the manuscript. All authors read and approved the final manuscript.

References
1. Gudiksen MS, Lauhon LJ, Wang J, Smith DC, Lieber CM: **Growth of nanowire superlattice structures for nanoscale photonics and electronics.** *Nature* 2002, **415**:617–620.
2. Yoon J, Jo S, Chun IS, Jung I, Kim HS, Meitl M, Menard E, Li XL, Coleman JJ, Paik U, Rogers JA: **GaAs photovoltaics and optoelectronics using releasable multilayer epitaxial assemblies.** *Nature* 2010, **465**:329–334.
3. Hou JJ, Han N, Wang F, Xiu F, Yip S, Hui AT, Hung T, Ho JC: **Synthesis and characterizations of ternary InGaAs nanowires by a two-step growth**

method for high-performance electronic devices. *ACS Nano* 2012, **6**:3624–3630.

4. del Alamo JA: **Nanometer-scale electronics with III-V compound semiconductors.** *Nature* 2011, **479**:317–323.

5. Dick KA, Caroff P, Bolinsson J, Messing ME, Johansson J, Deppert K, Wallenberg LR, Samuelson L: **Control of III-V nanowire crystal structure by growth parameter tuning.** *Semicond Sci Technol* 2010, **25**:024009.

6. Joyce HJ, Wong-Leung J, Gao Q, Tan HH, Jagadish C: **Phase perfection in zinc blende and wurtzite III − V nanowires using basic growth parameters.** *Nano Lett* 2010, **10**:908–915.

7. Krogstrup P, Popovitz-Biro R, Johnson E, Madsen MH, Nygård J, Shtrikman H: **Structural phase control in self-catalyzed growth of GaAs nanowires on silicon (111).** *Nano Lett* 2010, **10**:4475–4482.

8. Persson AI, Larsson MW, Stenstrom S, Ohlsson BJ, Samuelson L, Wallenberg LR: **Solid-phase diffusion mechanism for GaAs nanowire growth.** *Nat Mater* 2004, **3**:677–681.

9. Plante MC, LaPierre RR: **Control of GaAs nanowire morphology and crystal structure.** *Nanotechnology* 2008, **19**:495603.

10. Caroff P, Dick K, Johansson J, Messing M, Deppert K, Samuelson L: **Controlled polytypic and twin-plane superlattices in III–V nanowires.** *Nat Nanotechnol* 2008, **4**:50–55.

11. Pankoke V, Kratzer P, Sakong S: **Calculation of the diameter-dependent polytypism in GaAs nanowires from an atomic motif expansion of the formation energy.** *Phys Rev B* 2011, **84**:075455.

12. Shtrikman H, Popovitz-Biro R, Kretinin A, Houben L, Heiblum M, Bukała M, Galicka M, Buczko R, Kacman P: **Method for suppression of stacking faults in wurtzite III − V nanowires.** *Nano Lett* 2009, **9**:1506–1510.

13. Thelander C, Caroff P, Plissard S, Dey AW, Dick KA: **Effects of crystal phase mixing on the electrical properties of InAs nanowires.** *Nano Lett* 2011, **11**:2424–2429.

14. Wallentin J, Ek M, Wallenberg LR, Samuelson L, Borgström MT: **Electron trapping in InP nanowire FETs with stacking faults.** *Nano Lett* 2012, **12**:151–155.

15. Schroer MD, Petta JR: **Correlating the nanostructure and electronic properties of InAs nanowires.** *Nano Lett* 2010, **10**:1618–1622.

16. Dhaka V, Haggren T, Jussila H, Jiang H, Kauppinen E, Huhtio T, Sopanen M, Lipsanen H: **High quality GaAs nanowires grown on glass substrates.** *Nano Lett* 2012, **12**:1912–1918.

17. Han N, Wang FY, Hui AT, Hou JJ, Shan GC, Xiu F, Hung TF, Ho JC: **Facile synthesis and growth mechanism of Ni-catalyzed GaAs nanowires on non-crystalline substrates.** *Nanotechnology* 2011, **22**:285607.

18. Fan ZY, Ho JC, Takahashi T, Yerushalmi R, Takei K, Ford AC, Chueh YL, Javey A: **Toward the development of printable nanowire electronics and sensors.** *Adv Mater* 2009, **21**:3730–3743.

19. Akiyama T, Haneda Y, Nakamura K, Ito T: **Role of the Au/GaAs (111) interface on the wurtzite-structure formation during GaAs nanowire growth by a vapor–liquid–solid mechanism.** *Phys Rev B* 2009, **79**:153406.

20. Dick KA: **A review of nanowire growth promoted by alloys and non-alloying elements with emphasis on Au-assisted III-V nanowires.** *Prog Cryst Growth Charact Mater* 2008, **54**:138–173.

21. Wacaser BA, Dick KA, Johansson J, Borgstrom MT, Deppert K, Samuelson L: **Preferential interface nucleation: an expansion of the VLS growth mechanism for nanowires.** *Adv Mater* 2009, **21**:153–165.

22. Han N, Wang F, Hou JJ, Xiu F, Yip S, Hui AT, Hung T, Ho JC: **Controllable p-n switching behaviors of GaAs nanowires *via* an interface effect.** *ACS Nano* 2012, **6**:4428–4433.

23. Johansson J, Dick K, Caroff P, Messing M, Bolinsson J, Deppert K, Samuelson L: **Diameter dependence of the wurtzite − zinc blende transition in InAs nanowires.** *J PhysChem C* 2010, **114**:3837–3842.

24. Akiyama T, Sano K, Nakamura K, Ito T: **An empirical potential approach to wurtzite-zinc-blende polytypism in group III-V semiconductor nanowires.** *Jpn J Appl Phys* 2006, **45**:L275–L278.

25. Dubrovskii V, Sibirev N: **Growth thermodynamics of nanowires and its application to polytypism of zinc blende III-V nanowires.** *Phys Rev B* 2008, **77**:035414.

26. Zhang GQ, Tateno K, Sanada H, Tawara T, Gotoh H, Nakano H: **Synthesis of GaAs nanowires with very small diameters and their optical properties with the radial quantum-confinement effect.** *Appl Phys Lett* 2009, **95**:123104.

27. De A, Pryor CE: **Predicted band structures of III-V semiconductors in the wurtzite phase.** *Phys Rev B* 2010, **81**:155210.

28. Zanolli Z, Fuchs F, Furthmüller J, von Barth U, Bechstedt F: **Model GW band structure of InAs and GaAs in the wurtzite phase.** *Phys Rev B* 2007, **75**:245121.

29. Guo H, Wen L, Li X, Zhao Z, Wang Y: **Analysis of optical absorption in GaAs nanowire arrays.** *Nanoscale Res Lett* 2011, **6**:1–6.

30. Benyoucef M, Rastelli A, Schmidt O, Ulrich S, Michler P: **Temperature dependent optical properties of single, hierarchically self-assembled GaAs/AlGaAs quantum dots.** *Nanoscale Res Lett* 2006, **1**:172–176.

31. Murayama M, Nakayama T: **Chemical trend of band offsets at wurtzite/zinc-blende heterocrystalline semiconductor interfaces.** *Phys Rev B* 1994, **49**:4710.

32. Passlack M, Hong M, Mannaerts J: **Quasistatic and high frequency capacitance–voltage characterization of Ga_2O_3–GaAs structures fabricated by in situ molecular beam epitaxy.** *Appl Phys Lett* 1996, **68**:1099.

33. Jabeen F, Rubini S, Martelli F, Franciosi A, Kolmakov A, Gregoratti L, Amati M, Barinov A, Goldoni A, Kiskinova M: **Contactless monitoring of the diameter-dependent conductivity of GaAs nanowires.** *Nano Research* 2010, **3**:706–713.

34. Lide DR: *CRC Handbook of Chemistry and Physics.* Boca Raton: CRC Press; 1993.

35. Mead CA: **Metal–semiconductor surface barriers.** *Solid State Electron* 1966, **9**:1023–1033.